Contributions to Geophysics and Geodesy Vol. 49/3, 2019 (229–247)

A least-squares minimization approach to interpret gravity anomalies caused by a 2D thick, vertically faulted slab

El-Sayed ABDELRAHMAN, Mohamed GOBASHY

Geophysics Department, Faculty of Science, Cairo University, Giza, Egypt;
e-mail: sayed5005@yahoo.com, bouguer3000@yahoo.com

Abstract: We present a least-squares minimization approach to estimate simultaneously the depth to and thickness of a buried 2D thick, vertically faulted slab from gravity data using the sample spacing – curves method or simply s-curves method. The method also provides an estimate for the horizontal location of the fault and a least-squares estimate for the density contrast of the slab relative to the host. The method involves using a 2D thick vertical fault model convolved with the same finite difference second horizontal gradient filter as applied to the gravity data. The synthetic examples (noise-free and noise affected) are presented to illustrate our method. The test on the real data (Central Valley of Chile) and the obtained results were consistent with the available independent observations and the broader geological aspects of this region.

Key words: gravity thick fault, depth and thickness solutions, s-curves method, least-squares method

1. Introduction

A number of simple model geometries have been used to model the gravitational effect of the vertical fault. Many previous workers have assumed an infinite vertical step and chosen a geometry where one or more semi-infinite thin horizontal sheets are terminated by a vertical fault plane (*Nettleton, 1942; Grant and West, 1965; Sharma and Vyas, l970; Geldart et al., 1966; Gupta, 1983; Blakely and Simpson 1986; Klingelé et al., l991; Abdelrahman et al., 2003; Abdelrahman and Essa, 2015*). *Gendzwill (1970)* examined a different scenario where the fault was represented by a horizontal slab that was divided into 3 regions. The fault itself was associated with the central region, with linear density distribution, limited by constant density of surrounded sectors. In this paper, we examine the use of a truncated thick slab to represent a vertical fault. We present a methodology for simultaneously

doi: 10.2478/congeo-2019-0012

estimating the depth to and thickness of the slab as well as the density contrast.

The gravitational effect of some simple bodies (e.g., sphere, horizontal cylinder, vertical cylinder) is of symmetrical shape (with respect to horizontal coordinates). On the other hand, the effect of vertical fault is asymmetrical in the direction of horizontal profile. If geological knowledge suggests that a horizontally layered sequence is present, and that the vertical throw of the interpreted fault is large compared to the depth to the layer with a density contrast relative to the host, it is safe to simplify the model under consideration to just a truncated horizontal slab on the upthrown side of the fault. A 2D approximation can be used when the strike length of the fault is greater than the depth to the top of the faulted slab. Despite very significant differences in mathematical complexity, the expressions for calculating gravity effects of thin and thick truncated horizontal slabs produce responses that are difficult to distinguish. We argue that a slab with finite thickness (i.e., the thick slab model) be used in preference to the thin slab model. We assume the 2D thick, vertically faulted slab is characterized by: 1) semi infinite thick slab, 2) a density contrast relative to the host density, 3) a thickness that is significant in relation to the depth of burial, 4) a strike length that is large relative to the depth of burial, 5) a truncated vertical plane where the plane is perpendicular to a profile of vertical gravity measurements, 6) equi-spaced measurements along the profile and all taken at the same elevation, and 7) a vertical throw which is large when compared with the depth of burial.

Several methods have been used to interpret gravity data due to faults. *Geldart et al. (1966)* described a method of interpreting 2D gravity data of a single bed that is cut by a flat fault plane of arbitrary dip angle, taking into account the bed in both the upthrown and downthrown blocks. *Sharma and Vyas (1970*) presented a graphical methodology to interpret gravity data of a 2D fault cutting a series of beds. *Parasnis (1973)* showed the application of a vertical fault model to various geological scenarios, and how the gravity data of one or more thick truncated 2D slabs can be used to model these geological situations. *Telford et al. (1976)* developed the equation for modeling a thick slab with a dipping truncation plane and describe the application even if the depth of overburden is less than about twice the thickness of the slab. However, most of these methods are highly subjec-

tive in determining the fault parameters and can not be applied directly to measured gravity data consisting of the combined effect of a local structure (2D thick, vertically faulted slab) and a regional polynomial of zero or first order, i.e., some preparatory work is necessary to isolate a residual from the input data.

On the other hand, numerical methods are widely used to interpret gravity data due to simple structures. *Gupta (l983)* developed a least-squares approach to depth determination from gravity data due to sphere, cylinder, and first horizontal gradient of gravity data due to a thin faulted layer. *Abdelrahman et al. (1987)* showed the effectiveness of the least-squares method in determining depths to a vertical step (thin plate approximation) and a horizontal cylinder from second vertical gradient maps by finding a solution of a non-linear equation in depth. *Abdelrahman and El-Araby (1993)* suggested a least-squares approach to depth determination from moving average residual gravity profiles.

Finally, continuous modeling methods are excellent in determining the depth and the thickness of a buried faulted structure from gravity data (*Talwani et al., l959; Tanner, 1967; Cordell and Henderson, l968*). In these methods, iterative 2D and 3D solutions of gravity data were suggested. Given girded gravity values and certain limited restrictions on the mass distribution, a 2D or 3D structural model can be calculated automatically from gravity data by successive approximations.

In the present paper, we describe a least-squares minimization approach to estimate simultaneously the depth to and the thickness of a buried 2D thick, vertically faulted slab from gravity data using a technique that is termed the "s-curves method". Our method involves using a 2D thick vertical fault model convolved with the same finite difference second horizontal gradient filter as applied to the gravity data. The method also provides an estimate for the horizontal location of the fault and a least-squares estimate for the density contrast of the slab relative to the host. The method is similar to Euler deconvolution, but it solves not only for depth to the source but also the thickness independently. A scheme for analysis of gravity data has been formulated to determine the model parameters of the 2D thick, vertically faulted slab. We apply the method to synthetic data with and without random noise, and tested it on a field example from Central Valley of Chile.

2. The method

The direct problem for the 2D vertical fault (or semi-infinite Bouguer slab) can be derived with reference to the solid angle concept and is given by *Telford et al. (1976)* as:

$$g(x,t,d) = 2G\sigma\left[x\,\ln\frac{\sqrt{x^2+(d+t)^2}}{\sqrt{x^2+d^2}} + \pi t/2 + \right. \\ \left. + (t+d)\,\mathrm{atan}\left(\frac{x}{d+t}\right) - d\,\mathrm{atan}\left(\frac{x}{d}\right)\right], \tag{1}$$

where $g(x,t,d)$ is the gravitational effect of the 2D vertical fault, d is the depth to the top of the slab, t is the thickness of the slab, x is the horizontal position coordinate, G is the gravitational constant, and σ is the density contrast of the slab. The 2D thick, vertically faulted slab model is shown in Fig. 1.

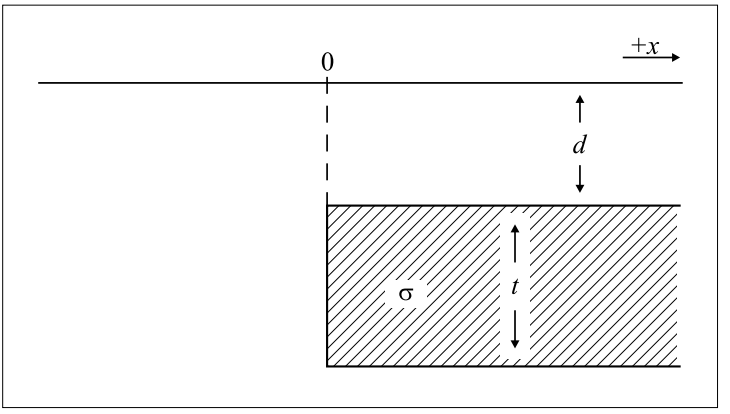

Fig. 1. Vertical schematic section through a 2D thick, vertically faulted slab. The fault is located at $x = 0$ on the horizontal coordinate axis. The slab has a thickness of t and the top of the slab is buried at a depth d. The slab has a density contrast of σ relative to the host density.

Consider five observation points $x_i + 2s$, $x_i + s$, x_i, $x_i - s$, and $x_i - 2s$ on the gravity profile where $s = k\,s_0$, $k = 1, 2, 3, ..., M$ spacing units and is called the graticule spacing and where s_0 is the fundamental sample spacing (*Hammer, 1977*). The numerical first horizontal gradient computed from gravity data is defined as:

$$g_x(x_i) = \frac{g(x_i + s) - g(x_i - s)}{2s}, \qquad i = 1, 2, 3, \ldots, N. \tag{2}$$

Using Eq. (2), the numerical second horizontal gradient computed from gravity data is then defined (*Levy, 2010*) as:

$$g_{xx}(x_i) = \frac{g(x_i + 2s) - g(x_i) + g(x_i - 2s)}{4s^2}. \tag{3}$$

Substituting (1) in (3), we obtain:

$$g_{xx}(x_i, t, d, s) = G\sigma W(x_i, t, d, s)/2s^2, \tag{4}$$

where

$$\begin{aligned} W(x_i, t, d, s) = {} & (x_i + 2s) \ln \frac{\sqrt{(x_i + 2s)^2 + (d + t)^2}}{\sqrt{(x_i + 2s)^2 + d^2}} + \\ & + (t + d) \operatorname{atan}\left(\frac{x_i + 2s}{t + d}\right) - d \operatorname{atan}\left(\frac{x_i + 2s}{d}\right) + \\ & - 2x_i \ln \frac{\sqrt{x_i^2 + (d + t)^2}}{\sqrt{x_i^2 + d^2}} - 2(t + d) \operatorname{atan}\left(\frac{x_i}{t + d}\right) + \\ & + 2d \operatorname{atan}\left(\frac{x_i}{d}\right) + (x_i - 2s) \ln \frac{\sqrt{(x_i - 2s)^2 + (d + t)^2}}{\sqrt{(x_i - 2s)^2 + d^2}} + \\ & + (t + d) \operatorname{atan}\left(\frac{x_i - 2s}{t + d}\right) - d \operatorname{atan}\left(\frac{x_i - 2s}{d}\right). \end{aligned} \tag{5}$$

Eq. (4) gives the following value at $x_i = s$:

$$g_{xx}(s) = G\sigma W(t, d, s)/2s^2, \tag{6}$$

where

$$\begin{aligned} W(t, d, s) = {} & 3s \ln \frac{\sqrt{9s^2 + (d + t)^2}}{\sqrt{9s^2 + d^2}} + (t + d) \operatorname{atan}\left(\frac{3s}{t + d}\right) + \\ & - d \operatorname{atan}\left(\frac{3s}{d}\right) - 3s \ln \frac{\sqrt{s^2 + (d + t)^2}}{\sqrt{s^2 + d^2}} + \\ & - 3(t + d) \operatorname{atan}\left(\frac{s}{t + d}\right) + 3d \operatorname{atan}\left(\frac{s}{d}\right). \end{aligned} \tag{7}$$

Using (6), (4) can be written as:

$$g_{xx}(x_i, t, d, s) = g_{xx}(s)\, W(x_i, t, d, s)/W(t, d, s)\,. \tag{8}$$

The unknown depth d in (8) can be obtained by minimizing:

$$\psi(d) = \min \|g_{xx}(x_i) - g_{xx}(s)\, W(x_i, t, d, s)/W(t, d, s)\|_2^2\,, \tag{9}$$

where $g_{xx}(x_i)$ represents the numerical second horizontal gradient computed from gravity data using Eq. (3) at x_i and where $g_{xx}(s)$ is a fixed numerical value at $x_i = s$ computed from the second horizontal gradient profile thus obtained, provided that the thickness t is known and remained constant in the process.

The minimization of the objective function is based on using the MATLAB function "lsqnonlin" which solves nonlinear least-squares problems of the form given in (9) (*Mathworks, 2018*). The "lsqnonlin" requires the user-defined function to compute the *vector*-valued function:

$$\psi(d) = \begin{bmatrix} \psi_1(d) \\ \psi_2(d) \\ \psi_3(d) \\ . \\ . \\ . \\ \psi_n(d) \end{bmatrix}. \tag{10}$$

Then, in vector terms, one can restate this optimization problem as:

$$\min_d \|\psi(d)\|_2^2 = \min_d \left(\psi_1(d)^2 + \psi_2(d)^2 + \psi_3(d)^2 + \ldots \psi_n(d)^2\right), \tag{11}$$

where d is a depth vector and $\psi(d)$ is a function that returns a vector value $d = \text{lsqnonlin}(\psi(d), d\_initial)$ starts at the depth $d\_initial$ (to be used only in the first iteration) and finds a minimum of the sum of squares of the functions described in $\psi(d)$. The minimization is performed using the Levenberg-Marquardt algorithm which uses a search direction that is a cross between the Gauss-Newton direction and the steepest descent direction. Any reasonable guess for d works well because there is only one minimum which is the global minimum (Fig. 2). In Fig. 2, we demonstrate an example of the objective function space when $s = 1\,\text{km}$, $t = 1\,\text{km}$, and initial guess of $d = 1\,\text{km}$ in case the model parameters are [$t = 9\,\text{km}$, $d = 5\,\text{km}$,

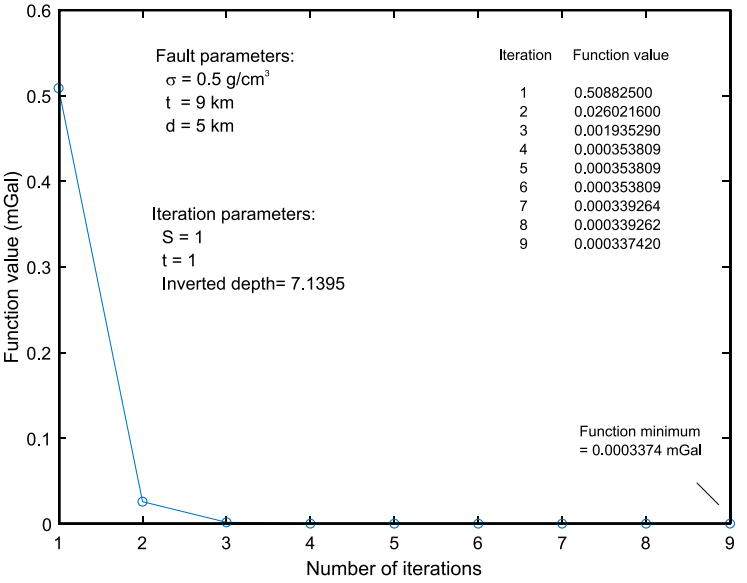

Fig. 2. A numerical example of the objective function space when $s = 1$ km, $t = 1$ km, and initial guess of $d = 1$ km in case the model parameters are: $t = 9$ km, $d = 5$ km, $\sigma = 0.5$ g/cm^3, profile length of 80 km, and sample interval of 1 km.

$\sigma = 0.5$ g/cm^3, profile length of 80 km, and sample interval of 1 km]. It is clear that among the function space, only one minimum is achieved at (iteration number 9) where the minimum is 0.0003374 mGal, which is at the same time as the global minimum. This shows that the function is generally concave and consequently the algorithm always converges to the minimum. In this case, any initial guess for d will work well.

Eq. (9) represents a parametric family of curves for different values of "s" (i.e., different sample spacings) and thus it can be used not only to determine depth d but also to estimate simultaneously the thickness of the buried fault t. For a fixed parameter s, the computed depths are plotted against the thickness values representing a continuous curve. The solution for the depth and the thickness of buried faulted slab is read at the common intersection of the curves. Theoretically, any two curves of the parameters are enough to simultaneously determine d and t. The curves intersect at the true values of d and t because (9) has only two unknowns. In practice, more than two values of graticule or sample spacing are desirable because

of the presence of noise in the data.

Finally, substituting the computed depth d_c and thickness t_c in (4) as fixed parameters and applying the least-squares method, we obtain the density contrast $\sigma(s)$ for any graticule spacing s as:

$$\sigma(s) = \sum \frac{2s^2 \left[g_{xx}(x_i)\, W(x_i, t_c, d_c, s)\right]}{G[W(x_i, t_c, d_c, s)]^2} \,. \tag{12}$$

The present method is capable of determining the model parameters, particularly the depth and the thickness of a buried thick vertically faulted slab from gravity data given in a small area over the buried structure, i.e., from a small segment of the gravity profile around the origin. In addition, the second horizontal gradient profiles exhibit a zero crossover at the origin (i.e., $x = 0$), hence, our method provides a simple way to estimate the horizontal location of the fault.

An automatic interpretation scheme based on the above equations for analyzing field data is as follows:

1) Digitize the anomaly profile at N data points.
2) Produce a set of second horizontal gradient profiles by applying the second horizontal gradient filter with different sample spacing values to the profile data set. The horizontal distance at which the second gradient profiles attain their zero value is taken as the origin of the gravity profile (i.e., $x = 0$). The default choice of the graticule spacing s is taken as $s = 5$ starting from $s = 1$ sampling interval.
3) For each second horizontal gradient profile, use (9) to determine the depth d of the buried fault structure for assumed values of thickness t. The default choice of the thickness values t is taken from 1 to 12 units every one sampling interval.
4) Construct the "s-curves" by plotting the computed depths against the thickness values for each s. The solution for the depth and thickness of buried faulted slab is read at the common intersection of the curves. The choice of the appropriate graticule spacings s) is based upon the resolution of the resulted intersected curves. If the intersection is not clear, the interpreter should use another set of graticule spacings (e.g. from s equals 6 to 10 sampling units).

A flowchart based on the above method for analyzing gravity data is shown in Fig. (3).

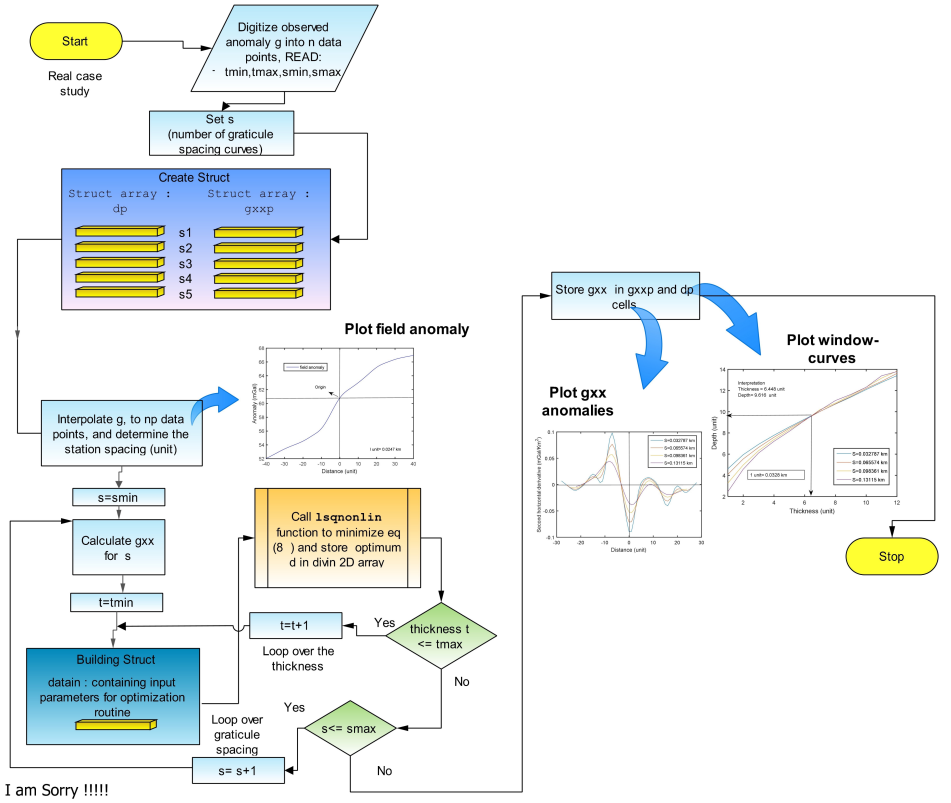

Fig. 3. A flowchart based on the present method for analyzing gravity data.

3. Theoretical examples

3.1. Noise free data

A composite synthetic example consisting of the combined gravity effect of a 2D thick, vertically faulted slab ($t = 9$ km, $d = 5$ km, $\sigma = 0.5$ g/cm^3, profile length $= 80$ km, and sample interval $= 1$ km) and a first-order regional polynomial (Fig. 4) was computed to allow us to demonstrate our method

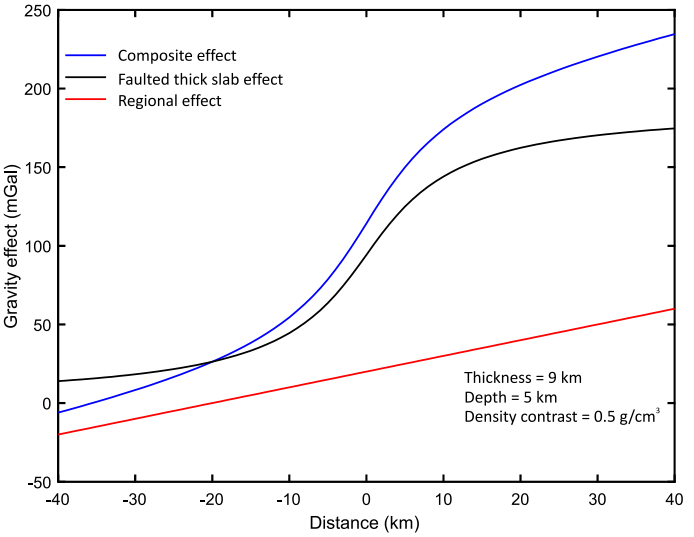

Fig. 4. A composite gravity profile consisting of the combined gravity effects due to a 2D thick vertically faulted slab ($t = 9$ km, $d = 5$ km, $\sigma = 0.5$ g/cm^3, profile length of 80 km, and sample interval of 1 km) and a regional component represented by a first-order polynomial.

for estimating the location, density contrast, depth to and thickness of the faulted thick slab. We produced profiles of the second horizontal gravity gradient using the discrete form of calculation (Eq. (3)) for values of the sample interval, s, of 1, 2, 3, 4, and 5 km (Fig. 5). The use of the second horizontal gradient filter has the effect of suppressing the longer wavelength components of the data in favor of the shorter wavelength components that are related to the buried truncated slab. Profiles for values of "s" greater than 5 km could have been calculated but the gradient profiles would continue to shrink in length due to the inability to calculate the result at locations close to either end of the profile.

Eq. (9) was applied to each point of the five-second horizontal gradient gravity profiles, yielding depth solutions for each of the thickness values that were proposed. The computed depths were plotted against the thickness values to produce the curves shown in Fig. 6. This figure shows the intersection at the correct location $t = 9$ km and $d = 5$ km. In this case, the solutions for the depth and thickness are in excellent agreement with the input model defined above.

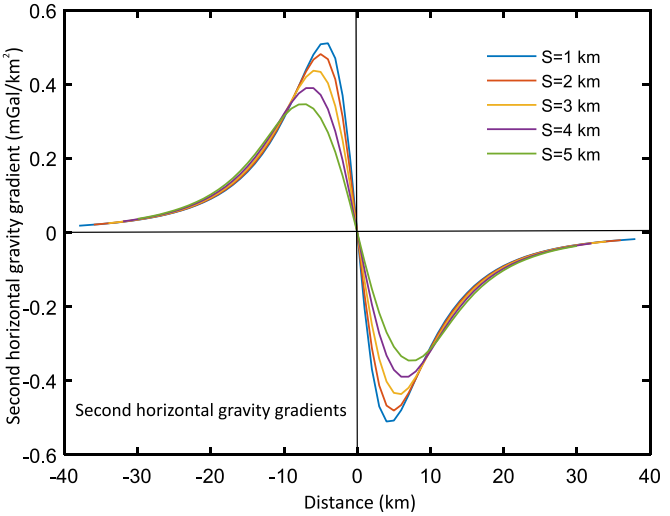

Fig. 5. Profiles of the discrete second horizontal gravity gradients for the composite field shown in Fig. 4. The gradients were calculated using a 3-point moving sampling spacing. The profiles represent the results that would be obtained using different gravity sample values (i.e., $s = 1, 2, 3, 4$, and 5 km).

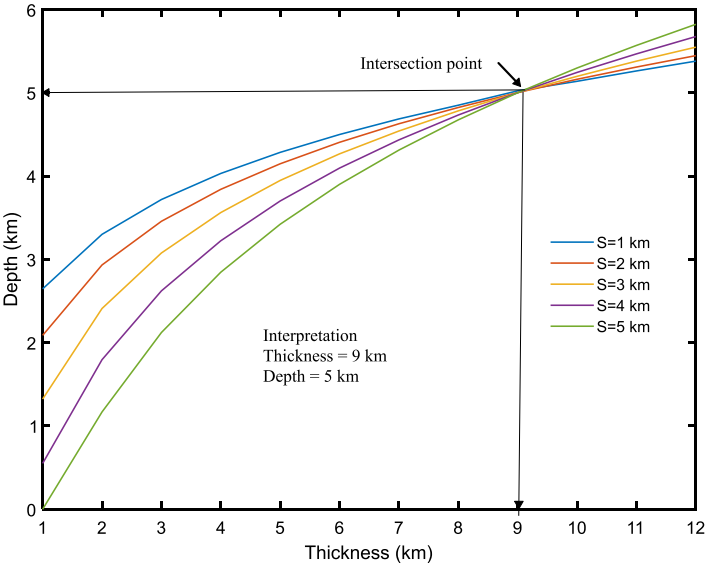

Fig. 6. Family of s-curves of thickness t as a function of depth to top d for sample interval s of 1, 2, 3, 4, and 5 km obtained from noise free composite gravity data using the present approach.

3.2. Effect of noise

The noise term in the measured signal, traditionally is related to the measurement errors (including instrumental errors). In the context of potential field analysis, two more types of noise are present, namely, earth noise (contribution from other neighboring undesired sources) and model errors (results from simplifying the real complex model). A common property of noise from all sources is the presence of significant power in the high frequency band. In the limiting case, we have white noise which has equal power in the entire frequency band of the observation (*Naidu and Mathew, 1998*). The measurement noise is more likely to be white noise. On the above basis, we implemented white noise in the simulation study. In our work, the "awgn" MATLAB function is used and the noise power is implemented. In this case, the SNR $= 20 \log_{10}(X^2/Y^2)$, where X represents the input signal and Y represents the noise. The SNR in the "awgn" function used specifies the (signal/noise) / sample in dB. The power used in "awgn" is measured from the input observed regularly spaced data $X(N)$. In this

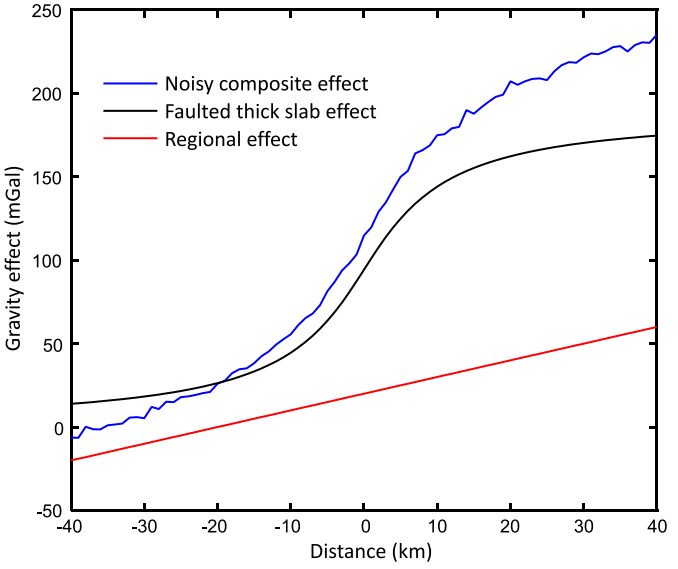

Fig. 7. A noisy composite gravity profile consisting of the combined effects due to a 2D thick, vertically faulted slab ($t = 9$ km, $d = 5$ km, $\sigma = 0.5$ g/cm^3 is the density contrast of the slab relative to the host, profile length $= 80$ km, and sample interval $= 1$ km) and a regional component represented by a first-order polynomial.

subsection, we investigate the effect of adding random noise.

The computed gravity effect of Fig. 4 was contaminated with 20 dB random noise (Fig. 7). The noisy composite gravity data thus obtained were subjected to the second horizontal gravity gradients filter to produce noisy second horizontal gravity gradients (Fig. 8). The second horizontal gravity gradients due to noisy data are more dominated in the right side of the Fig. 8 as compared to the left side. This is due to the fact the truncated slab is located below the positive profile values w.r.t. the start profile, i.e. zero crossing where the main part of the gravity effect of the truncated slab is emphasized. The gravity data below the positive is greatly affected by the second horizontal gradient filter compared with gravity data located below the negative profile side. Adapting the same interpretation technique described above, the results are shown in Fig. 9. The "s-curves" intersect each other at the location $t = 8.85$ km and $d = 4.94$ km. This demonstrates that our method can give reliable results even when the gravity data contains measurement errors or geological noise.

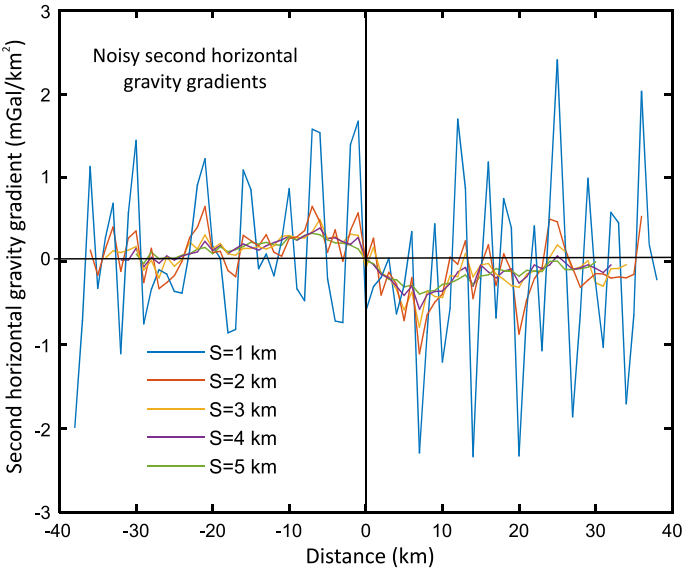

Fig. 8. Profiles of the discrete noisy second horizontal gravity gradients for the composite field shown in Fig. 7. The gradients were calculated using a 3-point sampling spacing. The profiles represent the results that would be obtained using different gravity sample values (i.e., $s = 1, 2, 3, 4,$ and 5 km).

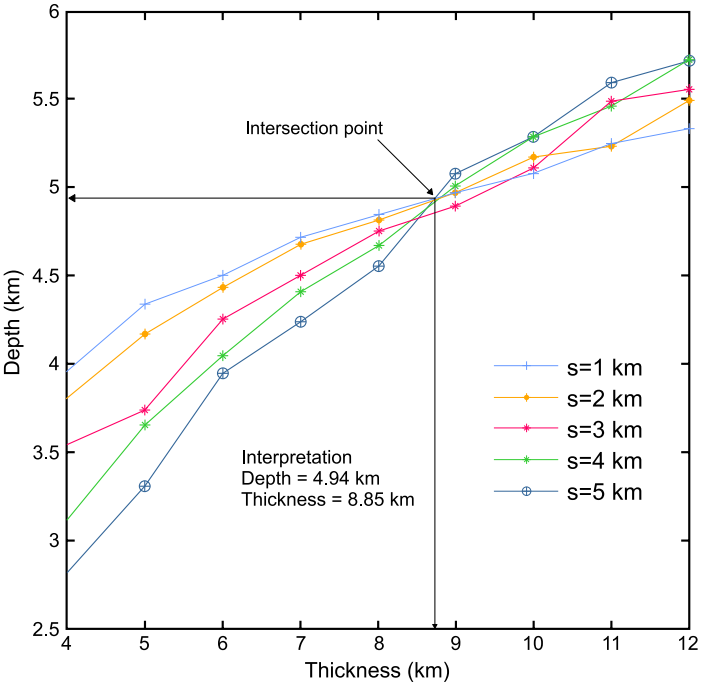

Fig. 9. Family of s-curves of t as a function of d for $s = 1, 2, 3, 4$, and 5 km as obtained from the noisy composite gravity data using the present approach.

4. Discussion

The present method assumes that the gravity data are regularly spaced and solution of Eq. 9) yields the exact value of depth and thickness when using synthetic data. Adding random noise to the synthetic data results in maximum uncertainties of ± 2.0 percent for parameters t and d.

For large s values, the number of samples on the second horizontal gradient curves decreases on both ends, which in turn may result in an instable interpretation curves. However, since the interpretation requires only a relatively short length profile, the problem may be solved effectively and economically by increasing the number of measurements made within the restricted length of the profile. At the same time, using a relatively short length of profile, results in a very high rejection of neighboring disturbances. The above explanation helps the user choose the proper s to use in Eq. (10).

The disadvantage of the present least-squares second horizontal gradient "*s*-curves" method is that it cannot be applied in complex geologic situations or areas with large-scale topographic and near-surface density variations. In this case, there is instability of the proposed inversion on the base of intersections of "*s*-curves".

5. Field example

To illustrate the practical application of the theory developed in the previous section, a field example from the Central Valley of Chile (*Garland, 1970*, the Figure 7.8, p. 116) is presented. A Bouguer anomaly profile across an outcropping fault structure in the basin is shown in Fig. 10 (*Lomnitz, l959*). The depth to the fault interpreted from surface geology and drilling information is about 0.15 km and the thickness estimated by *Lomnitz (l959)* using the Bouguer formula for a slab is about 2 km. The gravity profile of 16.55 km length has been digitized at an interval of 0.207 km. The Bouguer gravity anomalies thus obtained have been subjected to a separation technique using the second horizontal gradient method. Filters were applied

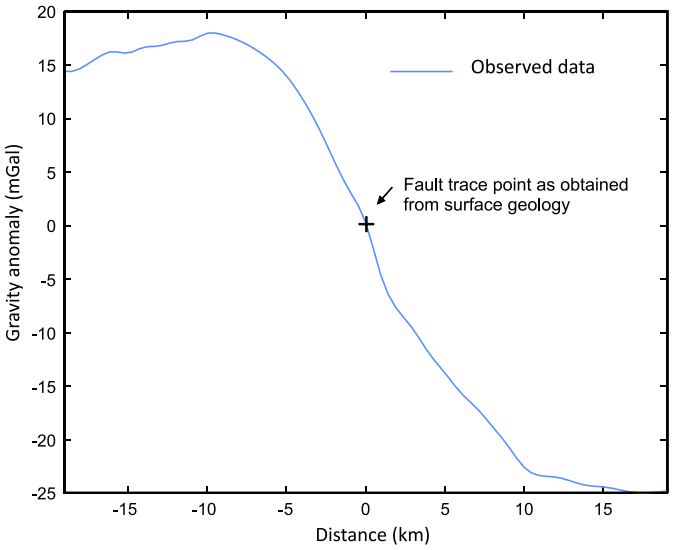

Fig. 10. Observed gravity anomaly over a 2D thick vertically faulted structure in the Central Valley of Chile (after *Lomnitz, l959*).

in four successive windows ($s = 2.482, 2.689, 2.896, 3.103$ km). In this way, four second horizontal gradient profiles were obtained (Fig. 11). The same procedure described for the synthetic examples was used to estimate the depth and the thickness of the fault. The results are shown in Fig. 12.

The result of the present study ($d = 0.19$ km and $t = 2.38$ km), based on the least-squares method, and that obtained from surface geology, drilling information, and application of the Bouguer formula for a horizontal slab are in a very good agreement.

6. Conclusions

The problem of determining the depth and the thickness of a 2D thick vertically faulted slab from second horizontal gradient gravity effects can be solved using the least-squares "s-curves" method described in this paper. The method involves fitting the response of a 2D thick vertical fault model convolved with the same second horizontal gradient filter as applied to the

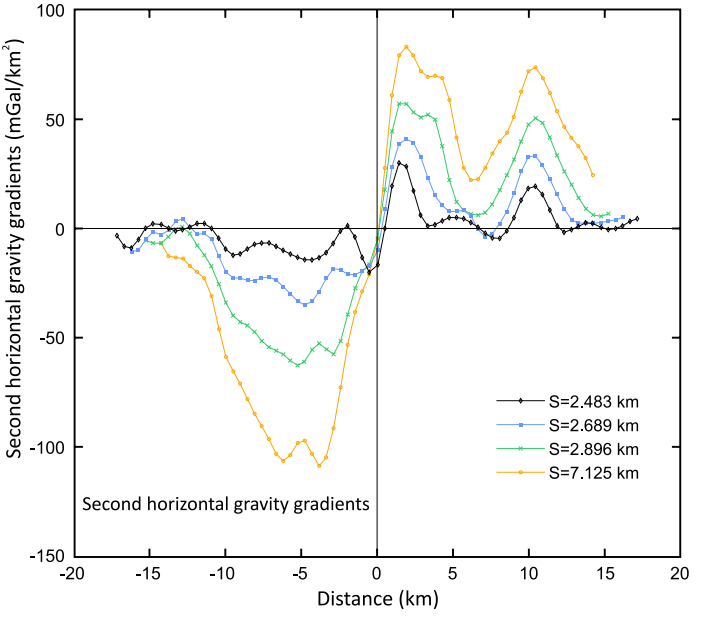

Fig. 11. Second horizontal gravity gradients due to a 2-D thick, vertically faulted structure, the Central valley of Chile for $s = 2.482, 2.689, 2.896, 3.103$ km.

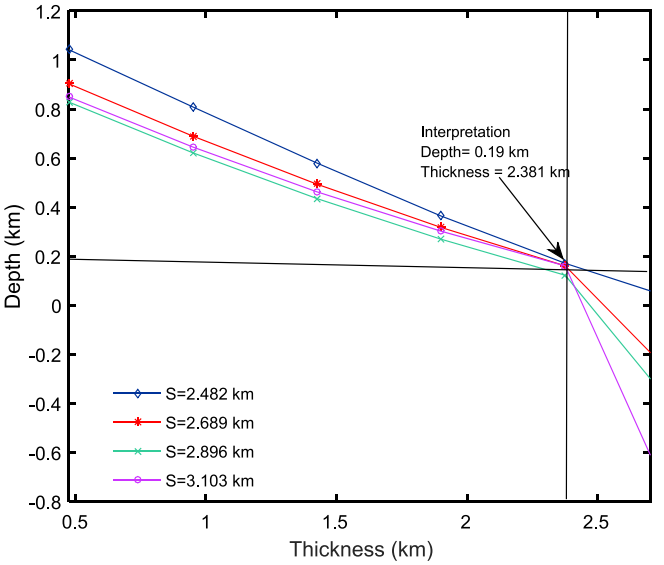

Fig. 12. Family of window curves of t as a function of d for $s = 2.482, 2.689, 2.896, 3.103$ km as obtained from the observed gravity anomaly due to a 2-D thick, vertically faulted structure, the Central valley of Chile, using the present approach.

observed data. Since the second horizontal gradient filter strongly attenuates any long wavelength regional component in the data, our method can be applied not only to data that have been pre-processed to remove a regional component but also to the measured Bouguer gravity data. The advantages of the present method over previous techniques are: (1) the least-squares "s-curves" method is a semi-automatic and computationally simple, and (2) the method is relatively stable when reasonable levels of noise is included in the observed data. The depth and thickness obtained by present method might be used to gain geologic insight concerning the subsurface. Synthetic and field examples illustrated the efficacy of the present method. The disadvantage of the present least-squares second horizontal gradient "s-curves" method is that it cannot be applied in complex geologic situations or areas with large-scale topographic and near-surface density variations.

Acknowledgements. The authors would like to thank the editors and the capable anonymous reviewer for their excellent suggestions and thorough review that improved our original manuscript.

References

Abdelrahman E. M., Bayoumi A. I., El-Araby H. M., 1987: A least-squares approach to depth determination from second derivative gravity anomalies due to two-dimensional faulted and folded structures with application to the Gulf of Suez region, Egypt. J. Afr. Earth Sci., **6**, 6, 857–860, doi: 10.1016/0899-5362(87)90044-3.

Abdelrahman E. M., El-Araby T., 1993: A least-squares minimization approach to depth determination from moving average residual gravity anomalies. Geophysics, **58**, 12, 1779–1784, doi: 10.1190/1.1443392.

Abdelrahman E. M., El-Araby H. M., El-Araby T. M., Abo-Ezz E. R., 2003: A least-squares derivatives analysis of gravity anomalies due to faulted thin slabs. Geophysics, **68**, 2, 535–543, doi: 10.1190/1.1567222.

Abdelrahman E. M., Essa K. S., 2015: Three least-squares minimization approaches to interpret gravity data due to dipping faults. Pure Appl. Geophys., **172**, 2, 427–438, doi: 10.1007/s00024-014-0861-4.

Blakely R. J., Simpson R. W; 1986: Approximating edges of source bodies from magnetic or gravity anomalies. Geophysics, **51**, 7, 1494–1498, doi: 10.1190/1.1442197.

Cordell L., Henderson R. G., 1968: Iterative three-dimensional solution of gravity anomaly data using a digital computer. Geophysics, **33**, 4, 596–601, doi: 10.1190/1.1439955.

Garland G. D.,l970: The earth's shape and gravity. Pergamon Press, 183 p.

Geldart L. P., Gill D. E., Sharma B.,1966: Gravity anomalies of two-dimensional faults. Geophysics, **31**, 2, 372–397, doi: 10.1190/1.1439781.

Gendzwill D. J., l970: The gradational density contrast as a gravity interpretation model. Geophysics, **35**, 2, 270–278, doi: 10.1190/1.1440090.

Grant F. S., West G. F., l965: Interpretation theory in applied geophysics. McGraw-Hill Book Co.

Gupta O. P., l983: A least-squares approach to depth determination from gravity data. Geophysics, **48**, 3, 357–360, doi: 10.1190/1.1441473.

Hammer S., l977: Graticule spacing versus depth discrimination in gravity interpretation. Geophysics, **42**, 1, 60–65, doi: 10.1190/1.1440714.

Klingelé E. E., Marson I., Kahle H.-G., 1991: Automatic interpretation of gravity gradimetric data in two dimensions: vertical gradient. Geophys. Prospect., **39**, 3, 407–434, doi: 10.1111/j.1365-2478.1991.tb00319.x.

Levy D., 2010: Introduction to numerical analysis. Maryland: Center for ScientificComputation and Mathematical Modeling, University of Maryland, p. 121.

Lomnitz C., l959: Gravimetric investigations in the Chillán region (Investigaciones gravimétricas en la región de Chillán). Boletín (Instituto de Investigaciones Geológicas (Chile)), **4**, Santiago de Chile, 19 p. (in Spanish).

Mathworks, 2018: MATLAB. http://mathworks.com/products/matlab/, accessed 27 February 2018.

Naidu P. S., Mathew M. P., 1998 : Analysis of geophysical potential fields, A digital signal processing approach. Advances in Exploration Geophysics, **5**, Elsevier Science, 8–9, eBook ISBN: 9780080527123, 297 p.

Nettleton L. L., 1942: Gravity and magnetic calculations. Geophysics, **7**, 3, 293–310, doi: 10.1190/1.1445015.

Parasins D. S., l973: Mining geophysics. Elsveier Scientific Publishing Co., ISBN: 9780444 601858.

Sharma B., Vyas M. P., 1970: Gravity anomalies of a fault cutting a series of beds. Geophysics, **35**, 4, 708–712, doi: 10.1190/1.1440124.

Talwani M., Worzel J. L., Landisman M., 1959: Rapid gravity computations for two-dimensional bodies with applications to the Mendocino submarine fracture zone. J. Geophys. Res., **64**, 1, 49–59, doi: 10.1029/JZ064i001p00049.

Tanner J. G., 1967: An automated method of gravity interpretation. Geophys. J. R. Astron. Soc., **13**, 1-3, 339–347, doi: 10.1111/j.1365-246X.1967.tb02164.x.

Telford W. M., Geldart L. P., Sheriff R. E., Key D. A., 1976: Applied Geophysics. Cambridge Univ. Press, London.